Research in Astron. Astrophys. **2012** Vol. **12** No. **5**, 573–583
http://www.raa-journal.org *http://www.iop.org/journals/raa*

***R**esearch in*
***A**stronomy and*
***A**strophysics*

The kinematics of an untwisting solar jet in a polar coronal hole observed by *SDO*/AIA *

Hua-Dong Chen[1,2], Jun Zhang[2] and Su-Li Ma[1,3]

[1] College of Science, China University of Petroleum, Qingdao 266555, China; *hdchen@upc.edu.cn*
[2] Key Laboratory of Solar Activity, National Astronomical Observatories, Chinese Academy of Sciences, Beijing 100012, China
[3] Harvard-Smithsonian Center for Astrophysics, MA 02138, USA

Received 2011 August 26; accepted 2012 January 16

Abstract Using the multi-wavelength data from the Atmospheric Imaging Assembly (AIA) onboard the *Solar Dynamics Observatory* (*SDO*) spacecraft, we study a jet occurring in a coronal hole near the northern pole of the Sun. The jet presented distinct upward helical motion during ejection. By tracking six identified moving features (MFs) in the jet, we found that the plasma moved at an approximately constant speed along the jet's axis. Meanwhile, the MFs made a circular motion in the plane transverse to the axis. Inferred from linear and trigonometric fittings to the axial and transverse heights of the six tracks, the mean values of the axial velocities, transverse velocities, angular speeds, rotation periods, and rotation radii of the jet are 114 km s^{-1}, 136 km s^{-1}, 0.81° s^{-1}, 452 s and 9.8×10^3 km respectively. As the MFs rose, the jet width at the corresponding height increased. For the first time, we derived the height variation of the longitudinal magnetic field strength in the jet from the assumption of magnetic flux conservation. Our results indicate that at heights of $1 \times 10^4 \sim 7 \times 10^4$ km from the base of the jet, the flux density in the jet decreases from about 15 to 3 G as a function of $B = 0.5(R/R_\odot - 1)^{-0.84}$ (G). A comparison was made with other results in previous studies.

Key words: Sun: activity — Sun: chromosphere — Sun: magnetic fields — Sun: flares — Sun: rotation

1 INTRODUCTION

Solar jets are small-scale plasma ejections along straight or slightly curved coronal fields (e.g. Shibata et al. 1994; Li et al. 1996; Chae et al. 1999). They can be observed as emission in ultraviolet (UV; e.g. Schmieder et al. 1988; Chen et al. 2008), extreme-ultraviolet (EUV; e.g. Schmahl 1981; Alexander & Fletcher 1999; Kamio et al. 2007; Kim et al. 2007; Chifor et al. 2008a,b; Kamio et al. 2009; Yang et al. 2011a; Tian et al. 2011), soft X-ray (SXR; e.g. Shibata et al. 1992; Zhang et al. 2000; Cirtain et al. 2007; Moore et al. 2011) and white light (WL; e.g. Wang et al. 1998a; Liu et al. 2005b). The detailed statistical properties of X-ray jets were studied by Shimojo et al.

* Supported by the National Natural Science Foundation of China.

(1996) and more recently by Savcheva et al. (2007). In terms of morphology, surges are very similar to jets, but they appear as absorption features when observed on solar disks. Sometimes, surges are observed to be associated with filament formation (e.g. Liu et al. 2005a), filament eruption (e.g. Chen et al. 2009a; Guo et al. 2010; Moore et al. 2010; Hong et al. 2011) and even coronal mass ejections (CMEs, e.g. Liu et al. 2005b; Jiang et al. 2008). Generally speaking, surges and jets are manifestations in different wavelengths of the same phenomenon. In the following context, we use the term "jets" to refer to both surges and jets.

Helical or twisted structures in jets have been reported by many authors (e.g. Dizer 1968; Shibata et al. 1992; Canfield et al. 1996; Wilhelm et al. 2002; Jibben & Canfield 2004; Jiang et al. 2007; Liu et al. 2009; Shen et al. 2011; Liu et al. 2011; Curdt & Tian 2011). By using line of sight velocity field (e.g. Xu et al. 1984; Gu et al. 1994; Jibben & Canfield 2004) and stereoscopic (e.g. Patsourakos et al. 2008; Nisticò et al. 2009) observations, some researchers confirmed that the rotational motions in some jets are real. Xu et al. (1984) proposed a double-pole diffusion model to explain the rotating motion of a surge. However, in consideration of the close relationship between jets and photospheric magnetic flux activities, such as magnetic flux emergence, convergence and cancellation (e.g. Roy 1973; Wang & Shi 1993; Shimojo et al. 1998; Zhang et al. 2000; Liu & Kurokawa 2004; Chen et al. 2008), more authors are inclined to think that the spinning of jets results from the relaxation of magnetic twist, which occurs when a twisted photospheric magnetic loop reconnects with ambient open fields (e.g. Shibata & Uchida 1986; Shibata et al. 1994; Canfield et al. 1996; Patsourakos et al. 2008; Nisticò et al. 2009; Kamio et al. 2010; He et al. 2010). Recently, three-dimensional simulations by Pariat et al. (2009) have shown that high-level magnetic stress due to twisting motion can lead to an explosive release of energy via reconnection, which will produce massive, high-speed jets driven by nonlinear Alfvén waves. If the stress is constantly applied at the photospheric boundary, this mechanism will generate recurrent untwisting quasi-homologous jets (e.g. Pariat et al. 2010; Asai et al. 2001; Chen et al. 2008; Yang et al. 2011b). More recently, the simulations by Díaz et al. (2011) have indicated that the speed of the flow along the field lines of twisted magnetic flux tubes may be super-Alfvénic, and the twisted tube is subject to kink instability, which could explain the behavior of super-Alfvénic jets and the disruption of some observed jets.

As mentioned above, so far the main observational methods to investigate the spinning of jets have focused on the analysis of the line of sight velocity field and stereoscopic observations, or taking advantage of the technique of time-distance analysis (e.g. Liu et al. 2009). The lower temporal and spatial resolutions of these observations, or the limitation of the technique used in these studies, cannot clearly discern the exact kinematics of the jet. For example, the tracks or stripes in the time-distance slit images cannot represent the real motion of jet plasma along the slit direction due to the perpendicular velocity. The Atmospheric Imaging Assembly (AIA; Lemen et al. 2011) on the Solar Dynamics Observatory (*SDO*; Schwer et al. 2002) images the solar atmosphere in 10 wavelengths with 12 s temporal resolution. The instrument observes solar plasma from the photosphere to the low corona with a full-disk field of view, and the pixel size is about $0.6''$. High-resolution AIA intensity images can reveal the fine structures in jets, which provides us with an opportunity to track the motions of some moving features (MFs) in jets. Using this new method, we study the detailed kinematics of one AIA 304 Å jet, which has been investigated by Shen et al. (2011) mainly using the time-distance slit image technique. One aim of this paper is to compare the results from the two different methods.

In addition, the measurement of coronal magnetic field strength is a long-standing unresolved problem in solar physics (e.g. West et al. 2011). Due to thermal broadening and the polarization effect, the usual methods for measuring coronal flux density, such as Zeeman splitting of spectral lines and the Hanle effect, become complicated. Focusing on the stronger active region fields, Lin et al. (2004) measured the magnetic flux density $100''$ ($\sim 7 \times 10^4$ km) above an active region to be 4 G, which is smaller than the results (10$\sim$33 G) presented by an earlier work from Lin et al. (2000). Some indirect methods, such as photospheric extrapolation techniques (e.g. Wang & Sheeley 1992;

Liu & Lin 2008), radio techniques (e.g. Ramesh et al. 2010) and coronal seismology (e.g. Uchida 1970; Roberts et al. 1984; Chen et al. 2011; West et al. 2011; Gopalswamy & Yashiro 2011), are applied to estimate the coronal magnetic field. In this study, in combination with the observations of the studied jet, we try to provide a new technique to estimate the magnetic field of the higher part of the jet, which would give valuable insight into the structure of the coronal magnetic field.

In the next section, we briefly describe the observations and data used in our study. This is followed by a detailed study of the kinematics of the jet and an estimation of the longitudinal magnetic flux density in the jet. Finally, we give the summaries and discussions.

2 DATA AND OBSERVATIONS

On 2010 August 21, a jet occurred at the northeast limb (E0N81) of the Sun (Shen et al. 2011). The observation from the Extreme UltraViolet Imager (EUVI; Wuelser et al. 2004) of the Sun Earth Connection Coronal and Heliospheric Investigation (SECCHI; Howard et al. 2008) onboard spacecraft B of the Solar Terrestrial Relations Observatory (STEREO; Kaiser et al. 2008), indicated that the jet is rooted in the coronal hole (e.g. Zhang et al. 2007) near the northern pole of the Sun. The detailed evolution of the jet was observed by the AIA on *SDO*, which provides multiple simultaneous high-resolution full-disk images up to $0.5R_{\odot}$ above the solar limb with 1.2 arcsec spatial resolution and 12 s cadence. All 10 bandpasses have been employed in the observations of this jet activity. In this paper, we mainly used the channels centered at 304 Å, 1600 Å, 171 Å, 193 Å and 211 Å (Level 1.5 images), with temperature response peaks at 0.05 MK, 0.1 MK, 0.6 MK, 1.5 MK (also 20 MK) and 2.0 MK, respectively (Lemen et al. 2011). We did not perform any de-rotation since the effect of rotation will not significantly influence our results.

3 RESULTS

3.1 General Evolution of the Jet

Figure 1 shows the morphology and general evolution of the jet at AIA 304 Å (reversed color table). Since the projected direction of the jet's axis is about 18° counterclockwise from the northern pole of the Sun, all the AIA images in this paper have been rotated by the same angle in a clockwise direction for better showing the features. According to the AIA observations, the jet took place at about 06:07 UT, when a brightening patch BP1 (see panel (a) of Fig. 1) first began to appear at one (eastern) side of the root and gradually evolved into an apparent inverted "Y" structure in the 171 Å images. From that point, dense plasma began to flow out from BP1 and expanded westwardly. From the AIA 1600 Å images, we can see that another brightening patch BP2 (in panel (a) of Fig. 1) appeared at the opposite (western) side of the base region at about 06:18 UT and peaked at 06:23 UT. In combination with the 304 Å observations, it seems that the main mass of the jet was ejected from above BP2 rather than BP1 after BP2 appeared. We consider that this location change of the jet footpoint has a close association with the magnetic reconnection occurring at the base of the jet.

As the plasma was ejected outwards, the jet also spun clockwise as viewed from its footpoints. Because of the movements along both the axial and transverse (rotation) direction, the jet appeared as upward helical structures. Some fine twisted threads with a mean width of a few arcseconds can be clearly identified, and are indicated by the white arrows in panels (e) and (f) of Figure 1. According to the chirality definition of jets in Jibben & Canfield (2004), the jet we studied here is a right-handed jet. As time went on, these threads gradually unwound, and one big bifurcation (indicated by the arrow in panel (g) of Fig. 1) appeared at about 06:35 UT from the bottom and spread upward along the body of the jet. At about 06:45 UT, after reaching a maximum height of 17.9×10^4 km, the material began to fall back almost along the axial direction without any transverse motion.

Interestingly, we note that another jet (indicated by the arrows in panels (i) and (j) of Fig. 1) occurred at about 06:42 UT, when the first had not yet completely disappeared. Its feet were very

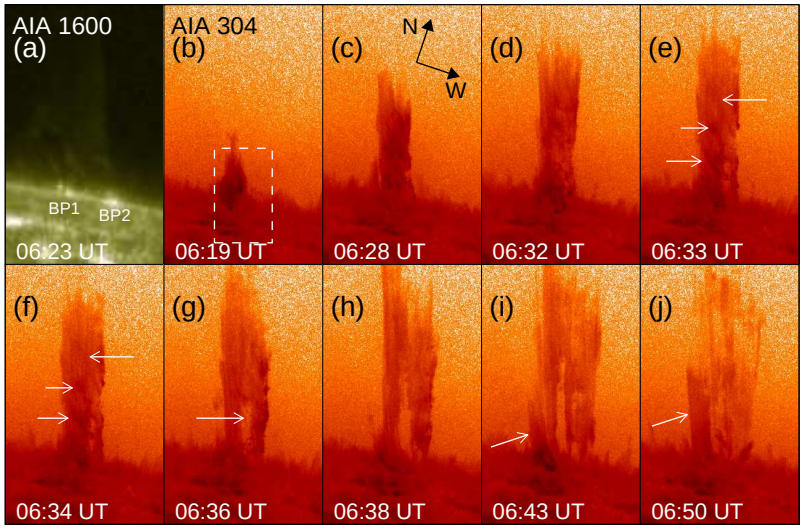

Fig. 1 Panel (a): AIA 1600 Å image displaying the brightening patches (BPs) at the base of the jet. Panels (b)–(j): negative AIA 304 Å images showing the detailed evolution of the jet. The images have been rotated in a clockwise direction by 18° from the northern pole of the Sun, which is the same for all AIA images in Figs. 2 and 3. The field of view (FOV) of the 304 Å images is $132'' \times 216''$. The dashed box in panel (b) indicates the FOV of panel (a), which is $48'' \times 79''$.

close to the feet of the first jet, which means they likely originated from the same source region. However, the ejection directions of the two jets were not very consistent with each other. A similar phenomenon has also been reported by Chen et al. (2008). In a recent simulation by Pariat et al. (2010), their results show that the drifting directions are different for recurrent jets, even if the underlying magnetic system and driving motion remain constant.

3.2 Helical Upward Motion

A remarkable character of this jet is its distinct transverse rotating motion. In Figure 2, we show this transverse motion in detail. Two AIA intensity images at 304 Å and 171 Å wavelengths are given in panels (a) and (c) of Figure 2, respectively. The three white narrow boxes ($74'' \times 4''$) in the 304 Å images mark three slits, S1-S3, from top to bottom, which are perpendicular to the jet axis. The heights of S1-S3 from the jet base are about 2.36×10^4, 4.43×10^4 and 6.50×10^4 km, respectively. In panel (b) of Figure 2, we display the time-distance diagrams at 304 Å along slits S1, S2 and S3 from top to bottom, respectively. As shown in these time-distance diagrams, it can be seen that there are many striped structures, which indicate the transverse motion of the plasma in the jet. In total, 15 stripes can be clearly identified in panel (b), among which several typical ones are indicated by the white arrows.

We performed linear fittings to all the 15 time-distance tracks, and found that the transverse velocities of these features range from 70 to 200 km s^{-1} with a mean value of 134 km s^{-1}. Using the same method, a more detailed investigation on the transverse motion of this jet has been done by Shen et al. (2011). According to their results, the total average transverse velocity of the jet is 123 km s^{-1}. In this paper, using the observations from other bandpasses, we further extended this study. In panel (d) of Figure 2, the time-distance diagrams from 171 Å, 193 Å, and 211 Å intensity images are plotted from top to bottom, respectively. Because the transverse rotation is not very

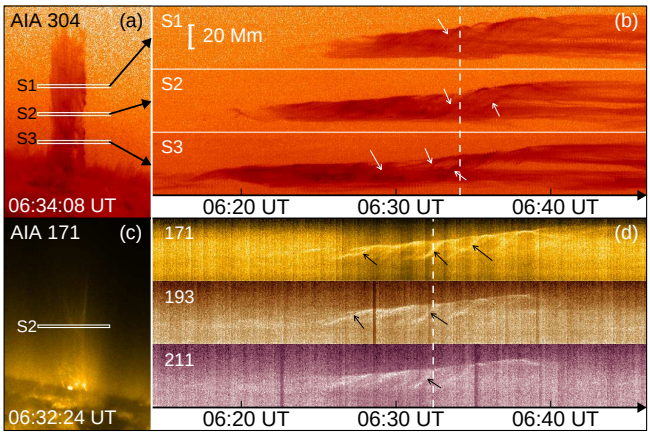

Fig. 2 Panels (a) and (c) are AIA 304 Å and 171 Å intensity images, respectively. They have the same FOV of $150'' \times 216''$. The white narrow boxes indicate the positions of slits S1-S3, which have an FOV of $74'' \times 4''$. Panel (b): slit images from the AIA 304 Å channel along S1-S3, respectively. Panel (d): slit images along S2 from the AIA 171 Å, 193 Å and 211 Å channels, respectively. The two white dashed lines indicate the times 06:34:08 and 06:32:24 UT when the AIA 304 Å and 171 Å intensity images (in panels (a) and (c), respectively) were recorded. The arrows in panels (b) and (d) point to some stripes, which indicate the transverse motions of the plasma across the jet.

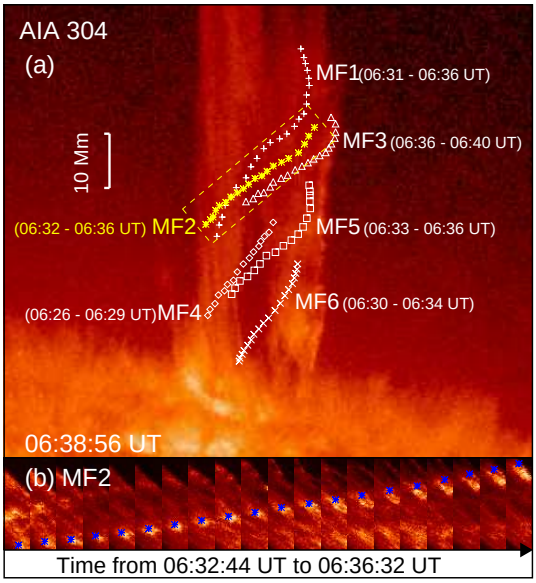

Fig. 3 Panel (a): one AIA 304 Å image overlaid with the tracks of MF1-MF6 (plus, asterisk, triangle, diamond, square and $\times$ symbols, respectively). The times in parentheses are the start and end tracking times of the corresponding MFs. The FOV of panel (a) is $168'' \times 144''$. The yellow dashed box indicates the FOV of the slit image in panel (b), which is about $14'' \times 52''$. Panel (b): slit images showing MF2. The blue asterisks indicate the positions of MF2 at different times.

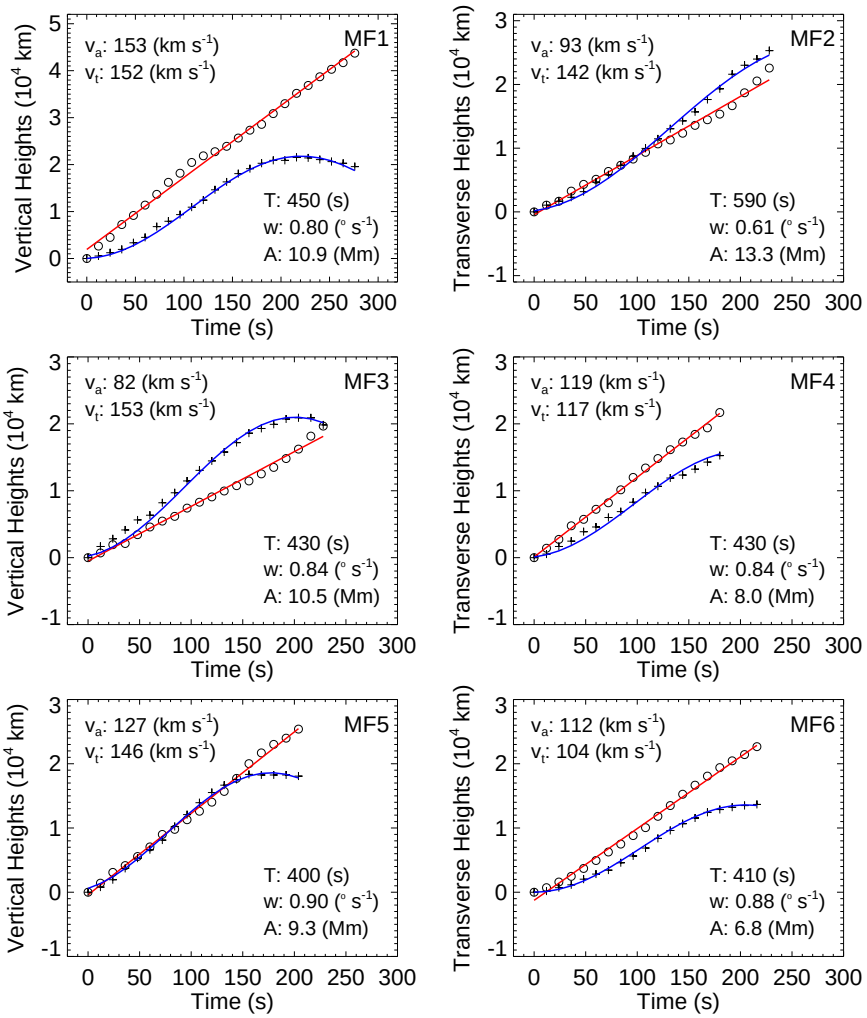

Fig. 4 Time variations of the relative axial (*circle*) and transverse (*plus*) heights of MF1-MF6. The red and blue solid lines are the results of linear and trigonometric fittings to the axial and transverse heights (*color online*), respectively. Here, $v_{\rm a}$, $v_{\rm t}$, T, ω and A represent the axial velocity, transverse velocity, rotation period, angular speed and rotation radius of the MFs, respectively.

clear in the 171 Å, 193 Å and 211 Å observations along S1 and S3, the time-distance diagrams at slit S2 are shown alone. Similarly, from the slit images in panel (d), the transverse helical motion features can be clearly identified, some of which are marked by the black arrows. Furthermore, in terms of morphology, these transverse motion features observed in the three EUV wavelengths are very similar. According to the linear fitting results, the mean transverse velocity of these features is around 140 km s^{-1}, which is similar to the result from the 304 Å slit images.

To reveal the kinematics of the jet more clearly, we tracked six moving features (MFs) that can be clearly identified in the jet. Considering the freezing-in effect of the plasma-magnetic field coupling, we assume that each MF moved along the same magnetic field line during ejection. In

panel (a) of Figure 3, one AIA 304 Å image at 06:38:56 UT is overlaid with the tracks of MF1-MF6 (marked with plus, asterisk, triangle, diamond, square and $\times$ symbols, respectively). The start and end of the tracking times of each MF are shown in the corresponding parentheses. It can be seen from Figure 3 that most of the MFs' tracks appear like helical lines, which indicates that the MFs made helical upward motions in the jet. As an example, we show the evolution of MF2 in panel (b) of Figure 3. The blue asterisks in panel (b) indicate the positions of MF2 at different times.

In Figure 4, we plot the time profiles of the axial (circle) and transverse (plus) heights of the six MFs. Note that the time and height in each panel are the values relative to the initial time and height of the respective MF. According to the different distributions of the axial and transverse heights, we can see that all the MFs seem to move at an approximately constant speed along the jet's axis and make a circular motion across the jet in the meantime. We performed linear (red solid line) and trigonometric (blue solid line) fittings to the axial and transverse heights of each MF, respectively. It can be found that the observational data are fitted very well, which provide further evidence of the helical motion of the jet. The axial velocity ($v_{\rm a}$), transverse velocity ($v_{\rm t}$), angular speed (ω), rotation period (T), and rotation radius (A) of each MF are derived from the linear and trigonometric fitting results and shown in the corresponding panel of Figure 4. The mean values of $v_{\rm a}$, $v_{\rm t}$, ω, T and A are 114 km s^{-1}, 136 km s^{-1}, 0.81° s^{-1} (or 14.1 $\times$ 10^{-3} rad s^{-1}), 452 s and 9.8 $\times$ 10^3 km, respectively. In comparison with the results from Shen et al. (2011), we found that most of the results are similar, except for the mean axial velocities, which are 114 and 171 km s^{-1} in our and their studies, respectively. This difference may result from the limitation of our sample number.

In addition, from the fitting results in our study, there seems to be no obvious correlation between $v_{\rm a}$ and $v_{\rm t}$. For example, the transverse velocities of MF1, MF2 and MF3 are about 150 km s^{-1}; however, the axial velocity (153 km s^{-1}) of MF1 is much larger than those (93 and 82 km s^{-1}) of MF2 and MF3. Of course, for a more accurate statistical relationship between the axial and transverse velocity of jet plasma, further study based on more samples is needed. Using these results, we roughly estimate the twist spreading into the outer corona during ejection, which might have previously been restored in the photospheric flux rope. The AIA 304 Å movie shows that the total spinning period of the jet is approximately from 06:16 UT to 06:42 UT ($\sim$26 minutes). Assuming that the jet made a uniform circular motion, the total restored twist can result from dividing the total spinning time by the mean rotation period (452 s), which is about 3.6 turns. In contrast to the result presented by Shen et al. (2011), ours is larger.

3.3 Axial Magnetic Field Strength in the Jet

As mentioned at the beginning, in this study we try to provide a new method to estimate the longitudinal magnetic field in the jet. Our basic idea is that assuming the jet plasma flows in the same flux tube during ejection, the magnetic flux across the transverse section of the jet would remain constant, i.e.

$$B_{\rm o}S_{\rm o} = BS. \tag{1}$$

So, if we can determine the photospheric magnetic field strength ($B_{\rm o}$), the transverse area ($S_{\rm o}$) of the flux tube at the jet base and the transverse area (S) of the flux tube at a certain height, then the axial magnetic field strength (B) at the corresponding height can be derived from Equation (1).

We describe the determinations of $B_{\rm o}$, $S_{\rm o}$, and S below. First, we think of the flux tube, the channel along which the jet material flows, as an approximately axisymmetric cylinder with an increasing radius (r). So, the transverse area $S_{\rm o}$ and S can be represented by $\pi r_{\rm o}^2$ and πr^2, respectively. Due to dispersion, it is difficult to measure the jet's radius ($r_{\rm o}$) at the base directly. Thus, $r_{\rm o}$ is estimated by the size of the brightening patch BP2 appearing at the jet base in the AIA 1600 Å image, which implies that $r_{\rm o}$ is about 2.6 $\times$ 10^3 km. By tracking the axial heights of the MFs at different times, we measured the width of the jet at the corresponding heights, which is twice the size of r. As for $B_{\rm o}$, since the jet occurred at the solar rim and there are no available photospheric magnetic

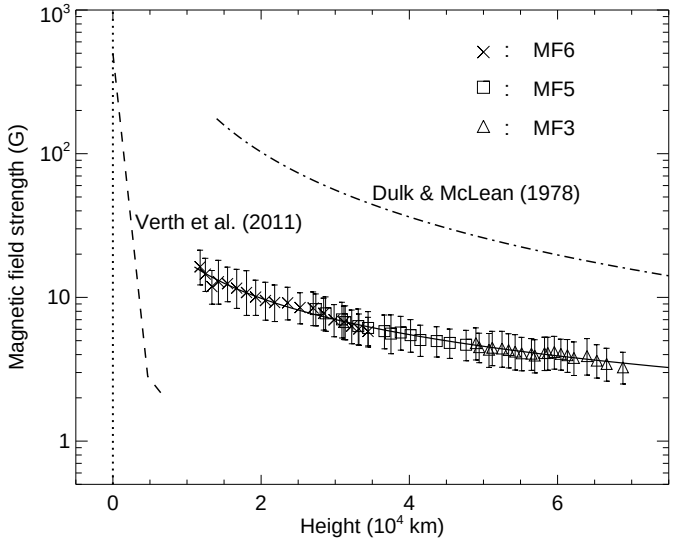

Fig. 5 The height variation of the axial magnetic field strength in the jet. The cross, square, and triangle symbols correspond to the data derived from the tracks of MF6, MF5 and MF3, respectively. The dashed and dash-dotted lines are the results from Verth et al. (2011) and Dulk & McLean (1978), respectively. The solid line is the fit to our observational data. The dotted line indicates the position of the solar surface.

field data, here we take the mean photospheric flux density value ($\sim$500 G) from Chen et al. (2008) as $B_{\rm o}$. Considering the similar spatial and temporal scales of the jets in this study and those in Chen et al. (2008), the value (500 G) of $B_{\rm o}$ that we used should be reasonable.

Using the corresponding data from the MF tracks, the axial magnetic field strength (B) along the jet was derived from Equation (1) and its variation with height (from the base of the jet) is shown in Figure 5. Note that we only used the data from three tracks of the MF3 (triangle), MF5 (square) and MF6 ($\times$). This is because it is not only the axial heights of the three MFs, but also their evolution times, that have better sequential data than the others (see Fig. 3). The errors from B mainly result from the uncertainty in the measurements of $r_{\rm o}$ and r and increase as the heights decline. From Figure 5, it can be seen that B decreases with increasing height. In particular, it falls quickly at the lower height. According to our results, B decreases by half (from about 15$\pm$4 to 7$\pm$2 G) from the height of 1.1 $\times$ 10^4 km to 2.8 $\times$ 10^4 km, with a mean drop rate of 4 G per 10^4 km. As the height keeps increasing, B gradually declines to about 3$\pm$1 G at a height of 7 $\times$ 10^4 km. From heights of 2.8 $\times$ 10^4 to 7 $\times$ 10^4 km, the mean decline rate of B is about 1 G per 10^4 km, which is only one fourth of that below 2.8 $\times$ 10^4 km.

Taking advantage of the same relationship of the magnetic flux density with the width of the flux tube, i.e. $B \sim 1/r^2$, Verth et al. (2011) studied the magnetic field strength along a solar spicule. Their results (dashed line) are shown in Figure 5. Obviously, the flux density derived in Verth et al. (2011) drops more quickly at the typical heights (from the photosphere to 7 $\times$ 10^3 km) of a spicule. As a comparison, we also show the results (dash-dotted line in Fig. 5) from the empirical active region magnetic field model (Dulk & McLean 1978), which is given by $B = 0.5(R/R_{\odot}\text{-}1)^{-1.5}$ G. On the whole, the field strength values from the model are about six times our results. In consideration of the different magnetic field structures between the above active region and in the coronal hole, and

the certainty of errors in measurement, we think that our results are reasonable. By slightly revising with the empirical formula presented by Dulk & McLean (1978), we found a new formula

$$B = 0.5(R/R_{\odot} - 1)^{-0.84} \ \mathrm{G}, \tag{2}$$

which fits our observations well, wherein, R is the distance from the solar center. In Figure 5, the fitting results are indicated by the black solid line across the different symbols.

4 SUMMARY

In this paper, we presented a detailed study of a jet which showed a distinct transverse rotating motion during its ejection. The observational results appear to be consistent with an untwisting model of magnetic reconnection (e.g. Shibata & Uchida 1986; Pariat et al. 2009, 2010). By tracking six identified features moving helically in the jet, we found that the jet plasma moved at an approximately constant velocity along the axial direction and made a circular motion in the plane perpendicular to the jet axis. We derived the axial velocity, transverse velocity, angular speed, rotation period and rotation radius for each MF. Their mean values are 114 km s^{-1}, 136 km s^{-1}, 0.81° s^{-1}, 452 s and 9.8 $\times$ 10^3 km , respectively. By comparison with the other study using a different method (Shen et al. 2011), we found that most of the results are similar. For more accurate kinematics of jet plasmas, more extensive statistical investigation work is expected in the future.

On assumption of the magnetic flux conservation in the same flux tube, we made an estimation of the field strength of the jet occurring in the polar coronal hole. Our results show that the longitudinal flux density of the jet at heights of $1 \times 10^4 \sim 7 \times 10^4$ km from the solar surface decreased from about 15 to 3 G. Comparing with the results from Dulk & McLean (1978), a new formula of $B = 0.5(R/R_{\odot}-1)^{-0.84}$ (G) fits our estimated data well. It should be noted that the B_{o} used in our study is just an estimated value, which may lead to a major error in the absolute value of B. However, this would not significantly affect the height variation of B. On the other hand, since almost all of the direct (Lin et al. 2000; Lin et al. 2004) or indirect (Cho et al. 2007; Ramesh et al. 2010; West et al. 2011) measurements of coronal field strength in previous studies are mainly focused on the stronger fields above, or at least which emanate from major active regions, our results could offer helpful information about magnetic field structures above the newly-emerging mini active regions in the coronal hole.

The formation of MFs in jets is also an interesting phenomenon. Similar features in jets can be seen in other observations (e.g. Jiang et al. 2007; Liu et al. 2009; Liu et al. 2011), although we know that both local density enhancement and temperature enhancement might be responsible for the existence of the MFs. However, why and how the local density or temperature enhancement takes place is still obscure at the present time. We suggest that three possible mechanisms might contribute to the formation of MFs. First, the formation of the MFs might be associated with the successive occurrence of magnetic reconnection at the base of the jet. Second, the intrinsic (sausage or kink) instability in the mass flow as described in Chen et al. (2009b) and Díaz et al. (2011) might be another possible candidate. In terms of morphology, MFs are similar to the plasma blobs observed in coronal streamers (e.g. Sheeley et al. 1997; Wang et al. 1998b; Wang et al. 2000; Song et al. 2009). The simulations by Chen et al. (2009b) reveal that the sausage-kink instability of coronal streamers may lead to the formation of plasma blobs, and at this point we think that the production mechanism of MFs in jets may be similar to that of the plasma blobs. In addition, the simulations of Díaz et al. (2011) support the theory that the kink instability in the mass flow can result in the disruption observed in solar jets. Finally, the intrinsic unevenness of the plasma density in the photospheric twisted flux tube might also be a possible formation mechanism of MFs in solar jets.

Acknowledgements The authors sincerely thank the anonymous referee for very helpful and constructive comments that improved this paper. We are grateful to all the members of the Solar

Magnetism and Activity group of National Astronomical Observatories of CAS for their invaluable help. We acknowledge the AIA team for easy access to the calibrated data. The AIA data are courtesy of *SDO* (NASA) and the AIA consortium. This work was supported by the National Natural Science Foundation of China (Grant Nos. 11103090, 11025315, 40890161, 10921303, 40825014, and 40890162), the CAS project KJCX2-YW-T04, the National Basic Research Program of China (973 Program, No. 2011CB811403), and the Shandong Provincial Natural Science Foundation, China (ZR 2011AQ009).

References

Alexander, D., & Fletcher, L. 1999, Sol. Phys., 190, 167
Asai, A., Ishii, T. T., & Kurokawa, H. 2001, ApJ, 555, L65
Canfield, R. C., Reardon, K. P., Leka, K. D., et al. 1996, ApJ, 464, 1016
Chae, J., Qiu, J., Wang, H., & Goode, P. R. 1999, ApJ, 513, L75
Chen, H., Jiang, Y., & Ma, S. 2009a, Sol. Phys., 255, 79
Chen, H. D., Jiang, Y. C., & Ma, S. L. 2008, A&A, 478, 907
Chen, Y., Feng, S. W., Li, B., et al. 2011, ApJ, 728, 147
Chen, Y., Li, X., Song, H. Q., et al. 2009b, ApJ, 691, 1936
Chifor, C., Isobe, H., Mason, H. E., et al. 2008a, A&A, 491, 279
Chifor, C., Young, P. R., Isobe, H., et al. 2008b, A&A, 481, L57
Cho, K.-S., Lee, J., Gary, D. E., Moon, Y.-J., & Park, Y. D. 2007, ApJ, 665, 799
Cirtain, J. W., Golub, L., Lundquist, L., et al. 2007, Science, 318, 1580
Curdt, W., & Tian, H. 2011, A&A, 532, L9
Díaz, A. J., Oliver, R., Ballester, J. L., & Soler, R. 2011, A&A, 533, A95
Dizer, M. 1968, Sol. Phys., 4, 99
Dulk, G. A., & McLean, D. J. 1978, Sol. Phys., 57, 279
Gopalswamy, N., & Yashiro, S. 2011, ApJ, 736, L17
Gu, X. M., Lin, J., Li, K. J., et al. 1994, A&A, 282, 240
Guo, J., Liu, Y., Zhang, H., et al. 2010, ApJ, 711, 1057
He, J.-S., Marsch, E., Curdt, W., et al. 2010, A&A, 519, A49
Hong, J., Jiang, Y., Zheng, R., et al. 2011, ApJ, 738, L20
Howard, R. A., Moses, J. D., Vourlidas, A., et al. 2008, Space Sci. Rev., 136, 67
Jiang, Y., Shen, Y., Yi, B., Yang, J., & Wang, J. 2008, ApJ, 677, 699
Jiang, Y. C., Chen, H. D., Li, K. J., Shen, Y. D., & Yang, L. H. 2007, A&A, 469, 331
Jibben, P., & Canfield, R. C. 2004, ApJ, 610, 1129
Kaiser, M. L., Kucera, T. A., Davila, J. M., et al. 2008, Space Sci. Rev., 136, 5
Kamio, S., Curdt, W., Teriaca, L., Inhester, B., & Solanki, S. K. 2010, A&A, 510, L1
Kamio, S., Hara, H., Watanabe, T., & Curdt, W. 2009, A&A, 502, 345
Kamio, S., Hara, H., Watanabe, T., et al. 2007, PASJ, 59, S757
Kim, Y.-H., Moon, Y.-J., Park, Y.-D., et al. 2007, PASJ, 59, S763
Lemen, J. R., Title, A. M., Akin, D. J., et al. 2011, Sol. Phys., 172
Li, K., Li, J., Gu, X., & Zhong, S. 1996, Sol. Phys., 168, 91
Lin, H., Kuhn, J. R., & Coulter, R. 2004, ApJ, 613, L177
Lin, H., Penn, M. J., & Tomczyk, S. 2000, ApJ, 541, L83
Liu, C., Deng, N., Liu, R., et al. 2011, ApJ, 735, L18
Liu, W., Berger, T. E., Title, A. M., & Tarbell, T. D. 2009, ApJ, 707, L37
Liu, Y., & Kurokawa, H. 2004, ApJ, 610, 1136
Liu, Y., Kurokawa, H., & Shibata, K. 2005a, ApJ, 631, L93
Liu, Y., & Lin, H. 2008, ApJ, 680, 1496

Liu, Y., Su, J. T., Morimoto, T., Kurokawa, H., & Shibata, K. 2005b, ApJ, 628, 1056
Moore, R. L., Cirtain, J. W., Sterling, A. C., & Falconer, D. A. 2010, ApJ, 720, 757
Moore, R. L., Sterling, A. C., Cirtain, J. W., & Falconer, D. A. 2011, ApJ, 731, L18
Nisticò, G., Bothmer, V., Patsourakos, S., & Zimbardo, G. 2009, Sol. Phys., 259, 87
Pariat, E., Antiochos, S. K., & DeVore, C. R. 2009, ApJ, 691, 61
Pariat, E., Antiochos, S. K., & DeVore, C. R. 2010, ApJ, 714, 1762
Patsourakos, S., Pariat, E., Vourlidas, A., Antiochos, S. K., & Wuelser, J. P. 2008, ApJ, 680, L73
Ramesh, R., Kathiravan, C., & Sastry, C. V. 2010, ApJ, 711, 1029
Roberts, B., Edwin, P. M., & Benz, A. O. 1984, ApJ, 279, 857
Roy, J. R. 1973, Sol. Phys., 28, 95
Savcheva, A., Cirtain, J., Deluca, E. E., et al. 2007, PASJ, 59, S771
Schmahl, E. J. 1981, Sol. Phys., 69, 135
Schmieder, B., Mein, P., Simnett, G. M., & Tandberg-Hanssen, E. 1988, A&A, 201, 327
Schwer, K., Lilly, R. B., Thompson, B. J., & Brewer, D. A. 2002, AGU Fall Meeting Abstracts, C1
Sheeley, N. R., Jr., Wang, Y.-M., Hawley, S. H., et al. 1997, ApJ, 484, 472
Shen, Y., Liu, Y., Su, J., & Ibrahim, A. 2011, ApJ, 735, L43
Shibata, K., Ishido, Y., Acton, L. W., et al. 1992, PASJ, 44, L173
Shibata, K., Nitta, N., Strong, K. T., et al. 1994, ApJ, 431, L51
Shibata, K., & Uchida, Y. 1986, Sol. Phys., 103, 299
Shimojo, M., Hashimoto, S., Shibata, K., et al. 1996, PASJ, 48, 123
Shimojo, M., Shibata, K., & Harvey, K. L. 1998, Sol. Phys., 178, 379
Song, H. Q., Chen, Y., Liu, K., Feng, S. W., & Xia, L. D. 2009, Sol. Phys., 258, 129
Tian, H., McIntosh, S. W., Rifal Habbal, S., & He, J. 2011, ApJ, 736, 130
Uchida, Y. 1970, PASJ, 22, 341
Verth, G., Goossens, M., & He, J.-S. 2011, ApJ, 733, L15
Wang, J., & Shi, Z. 1993, Sol. Phys., 143, 119
Wang, Y.-M., Sheeley, N. R., Socker, D. G., Howard, R. A., & Rich, N. B. 2000, J. Geophys. Res., 105, 25133
Wang, Y.-M., & Sheeley, N. R., Jr. 1992, ApJ, 392, 310
Wang, Y.-M., Sheeley, N. R., Jr., Socker, D. G., et al. 1998a, ApJ, 508, 899
Wang, Y.-M., Sheeley, N. R., Jr., Walters, J. H., et al. 1998b, ApJ, 498, L165
West, M. J., Zhukov, A. N., Dolla, L., & Rodriguez, L. 2011, ApJ, 730, 122
Wilhelm, K., Dammasch, I. E., & Hassler, D. M. 2002, Ap&SS, 282, 189
Wuelser, J.-P., Lemen, J. R., Tarbell, T. D., et al. 2004, in Society of Photo-Optical Instrumentation Engineers (SPIE) Conference Series 5171, eds. S. Fineschi, & M. A. Gummin, 111
Xu, A.-A., Yin, S.-Y., & Ding, J.-P. 1984, Acta Astronomica Sinica, 25, 119
Yang, L.-H., Jiang, Y.-C., Yang, J.-Y., et al. 2011a, RAA (Research in Astronomy and Astrophysics), 11, 1229
Yang, S., Zhang, J., Li, T., & Liu, Y. 2011b, ApJ, 732, L7
Zhang, J., Wang, J., & Liu, Y. 2000, A&A, 361, 759
Zhang, J., Zhou, G., Wang, J., & Wang, H. 2007, ApJ, 655, L113